

飞秒激光辐照氧化石墨烯的纳结构与电化学性能研究

李强^{1,2}, 丁烨^{1,2*}, 杨立军^{1,2**}, 王扬^{1,2}

¹ 教育部微系统与微结构制造重点实验室, 黑龙江 哈尔滨 150001;

² 哈尔滨工业大学机电工程学院, 黑龙江 哈尔滨 150001

摘要 氧化石墨烯的还原与表面结构化有助于提升传感器、储能器等微型电子器件的性能。相比于其他工艺手段,采用飞秒激光辐照方法可以快速实现氧化石墨烯的同步还原和表面纳结构成型。本文首次对比了 1030 nm 和 257 nm 两种飞秒激光波长辐照下氧化石墨烯的形貌与结构特征,发现 1030 nm 激光辐照产生的条纹周期纳结构主要由入射激光与表面等离激元干涉作用而形成,257 nm 激光辐照产生的沟槽微纳结构主要归因于光化学作用。通过拉曼测试和电化学阻抗谱分析表明,相比于 257 nm 激光作用,1030 nm 激光辐照下氧化石墨烯还原程度更高,电极反应过程中接触电阻更小且有利于电荷转移和离子的扩散。

关键词 激光技术; 飞秒激光; 氧化石墨烯; 纳结构; 电化学性能

中图分类号 O439

文献标志码 A

doi: 10.3788/CJL202148.0802022

1 引言

石墨烯由于其高导电性、高热导率和高比表面积的优势^[1-3],逐步成为柔性储能器件^[4]和传感器^[5]等领域研究热点。相比于化学气相沉积^[6]、石墨机械剥离^[7]和外延生长^[8]等方法,氧化石墨烯还原更易于满足实际生产对于石墨烯产量的需求。目前氧化石墨烯还原的方式主要以化学还原^[9]、热还原^[10]和光还原^[11]为主,从还原方法的效率和可控性角度看,采用激光辐照方法^[12-14]可以在不需要特殊的物理或化学条件下,直接去除表面的含氧官能团,实现氧化石墨烯的快速还原,因此被认为是最具优势的石墨烯制备方法。

近年来,针对激光还原氧化石墨烯也进行了广泛的研究。Guo 等^[15]利用双束激光干涉方法同步还原和表面刻划氧化石墨烯,通过改变入射激光功率,可以方便地控制氧化石墨烯的还原程度和表面形貌特征,并且基于所获得的多级形貌结构的激光还原氧化石墨烯,成功制备出具有快速响应率和灵敏度的柔性湿度传感器。Kang 等^[16]详细研究了连

续激光和飞秒激光对于氧化石墨烯还原的影响,发现脉冲频率 10 kHz 的飞秒激光辐照更有助于还原氧化石墨烯的电导率提升,非线性的光化学作用对于氧原子去除起主导作用,凭借这种方法可以实现石墨烯薄膜的快速制备和无损伤加工。Trusovas 等^[17]采用皮秒激光辐照氧化石墨方法,研究了还原氧化石墨烯的特征拉曼峰的面积和位置变化,结果表明,当入射激光功率为 50 mW,扫描速度为 30 mm/s 时,表面结构缺陷最小且还原程度最高,此外他们还进一步分析了激光还原氧化石墨过程中温度场的变化,认为辐照局部产生 1200 K 左右的高温有助于表面含氧官能团的去除。Kasischke 等^[18]分析了在超快激光辐照过程中还原氧化石墨烯表面形貌演变特征与化学成分变化,他们认为超快激光与氧化石墨烯作用中自组装效应直接导致了表面周期结构的成型,采用这种方法可以同步获得带有周期结构的还原氧化石墨烯。但是直到目前,人们对于飞秒激光还原氧化石墨烯的研究还不足,表面纳结构形貌和结构特征尚需要进一步探究。因此,本文主要针对氧化石墨烯的飞秒激光纳结构成型与电

收稿日期: 2020-12-02; 修回日期: 2020-12-29; 录用日期: 2021-02-08

基金项目: 国家重点研发计划(2017YFB1104900)、中国博士后科学基金(2020M670900)、黑龙江省博士后面上资助(LBH-Z20054)

* E-mail: dy1992hit@hit.edu.cn; ** E-mail: yljtj@hit.edu.cn

化学阻抗特性开展研究,分析入射激光的波长、脉冲个数和能量对于氧化石墨烯烧蚀特性的影响,对比1030 nm和257 nm波长的激光辐照产生的纳结构形貌与结构特征,进一步探讨不同表面纳结构对于电化学阻抗特性的影响。

2 实验方法

在进行飞秒激光超快作用氧化石墨烯实验之前,首先需要制备氧化石墨烯薄膜。基于常用的Hummers方法^[19],首先在干燥的烧杯中加入适量的浓硫酸(H_2SO_4 ,体积分数为98%),搅拌过程中加入石墨粉(2 g)和硝酸钠粉末(1 g),再依次加入高锰酸钾($KMnO_4$,6 g),搅拌并控制温度不超过20 °C,继续搅拌并升温至35 °C保持2 h。然后

缓慢加入去离子水,通过适量的双氧水(H_2O_2)还原残余的氧化剂,洗涤并过滤烘干。结合真空冷却方式获得氧化石墨烯粉末。相比于石墨烯,氧化石墨烯表面和边缘处含有大量的含氧官能团(羟基、羧基等),使其具有很好的亲水性,易于制备不同浓度的分散液,因此采用超声喷涂方法可以获得厚度均匀的氧化石墨烯薄膜。首先将200 mg的氧化石墨烯粉末溶解到100 mL的去离子水中,超声分散3 h后获得质量浓度为2 mg/mL的氧化石墨烯分散液。喷涂基底选择聚对苯二甲酸乙二醇酯(PET)薄膜,为了保证喷涂薄膜表面的一致性,喷涂过程中需要控制流量和次数,表1给出了喷涂薄膜的具体参数,图1为氧化石墨烯薄膜的表面与侧面形貌。

表1 喷涂氧化石墨烯薄膜的参数

Table 1 Parameters of graphene oxide by spray coating

Parameter	Flow velocity / ($mL \cdot min^{-1}$)	Gas pressure / MPa	Temperature / °C	Spraying number
Value	0.2	0.03	48~50	100

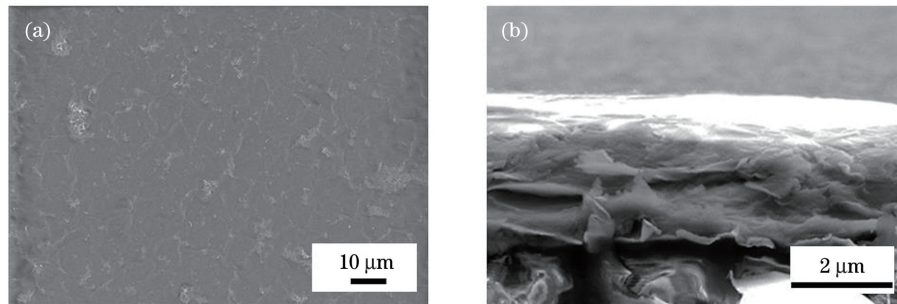


图1 氧化石墨烯薄膜的形貌。(a) 表面形貌;(b)侧面形貌

Fig. 1 Morphology of graphene oxide film. (a) Surface morphology; (b) lateral morphology

所使用的飞秒激光微细加工系统构成如图2所示。系统主要包括了飞秒激光器(Pharos, L15400)、

偏振调节装置、三维移动平台和视觉检测系统等。飞秒激光器通过倍频模块能够输出三个波长,分别

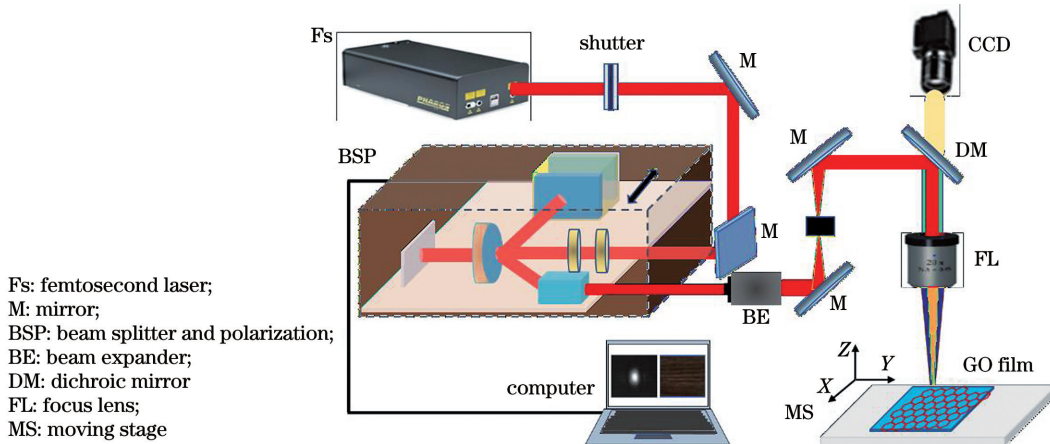


图2 飞秒激光辐照氧化石墨烯的系统原理图

Fig. 2 Schematic illustration of the graphene oxide by femtosecond laser irradiation

为基频(1030 nm)、二倍频(515 nm)和四倍频(257 nm),最小脉冲宽度可达255 fs,脉冲放大器输出的重复频率为1 kHz~1.1 MHz,脉冲能量最大为440 μJ且可以实现单脉冲触发。由于激光器输出光为线偏振,通过偏振调节装置可以改变飞秒激光的偏振方向。氧化石墨烯薄膜固定在三维微移动平台上,平台的定位精度为1 μm。采用扫描电子显微镜(Zeiss Merlin Compact)观察飞秒激光辐照氧化石墨烯表面纳结构形貌,拉曼光谱测试表征激光辐照后氧化石墨烯的还原程度与结构特征。飞秒激光在还原氧化石墨烯薄膜表面刻划出插指形状电极,电解液选用聚乙烯醇/硫酸配置而成的凝胶电解质。电极的电化学阻抗特性通过电化学工作站(Autolab, PGSTA302N)测试获得。

3 分析与讨论

3.1 氧化石墨烯的烧蚀特性

在研究飞秒激光辐照氧化石墨烯表面纳结构成型之前,首先针对氧化石墨烯在不同入射激光参数下的烧蚀特性进行分析。烧蚀试验采用激光单点辐照方法,通过控制激光辐照的脉冲能量和脉冲个数,分析氧化石墨烯表面烧蚀特性。为了避免过高的激光能量,导致氧化石墨烯基底的损伤。试验过程中辐照的激光脉冲能量低于100 nJ,脉冲个数在5~100范围内。最终激光辐照所形成的表面形貌利用扫描电子显微镜(SEM)观察获得。

图3为1030 nm波长的飞秒激光辐照下,氧化石墨烯表面烧蚀区域面积与入射脉冲个数以及脉冲能量的变化关系。可以看出,当脉冲能量一

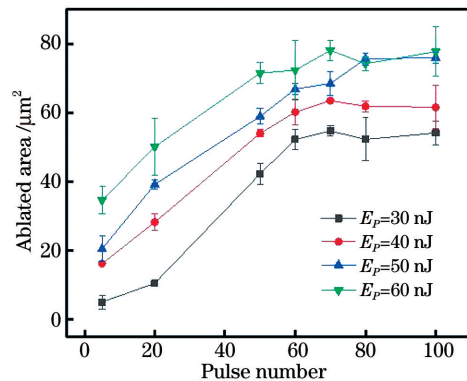


图3 1030 nm 波长激光辐照下氧化石墨烯的烧蚀区域面积演变

Fig. 3 Evolution of the ablated area of graphene oxide by 1030 nm femtosecond laser irradiation

定时,烧蚀区域面积大小随辐照的脉冲个数的增加呈现出不同的变化趋势。在脉冲个数为5~60时,氧化石墨烯烧蚀区域面积变化以线性增加为主,而脉冲个数超过60时,烧蚀区域面积变化不大,表明氧化石墨烯烧蚀区域面积的增加不与辐照的脉冲个数呈线性关系。结合图4中氧化石墨烯在40 nJ脉冲能量辐照下表面烧蚀形貌的演变,发现不同脉冲个数辐照后烧蚀形貌有很大差别。在脉冲个数为5时,辐照区域边缘均匀分布着纳米薄片,并且区域内部出现了类似于层状的纳米结构;随着入射脉冲个数的增加,边缘的纳米薄片更加明显,与此同时烧蚀区域深度也随之增加。对比脉冲个数为20和100时激光烧蚀表面形貌,可以发现在多脉冲辐照下,烧蚀区域内部呈现环状分层形貌,环状边缘也分布着明显的纳米条纹结构。

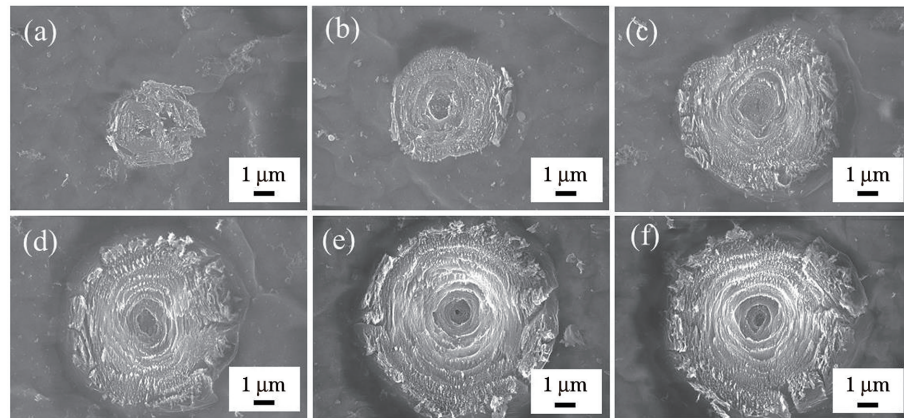


图4 1030 nm 飞秒激光辐照下氧化石墨烯表面烧蚀形貌。(a) 5脉冲;(b) 20脉冲;(c) 50脉冲;(d) 60脉冲;(e) 80脉冲;(f) 100脉冲;

Fig. 4 Ablated surface morphology of graphene oxide by 1030 nm femtosecond laser irradiation. (a) 5 pulses; (b) 20 pulses; (c) 50 pulses; (d) 60 pulses; (e) 80 pulses; (f) 100 pulses

应该指出,激光烧蚀的表面形貌特征与入射波长有关。图5描述了257 nm飞秒激光辐照下,氧化石墨烯的烧蚀区域面积演变。

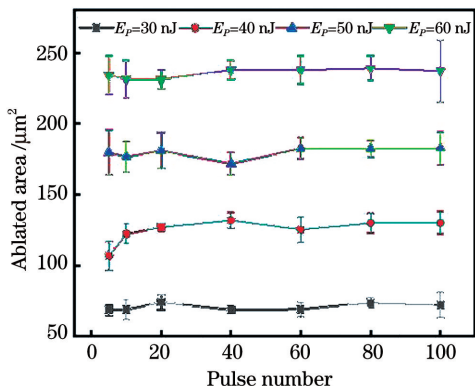


图5 257 nm 波长激光辐照下氧化石墨烯的烧蚀区域面积演变

Fig. 5 Evolution of the ablated area of graphene oxide by 257 nm femtosecond laser irradiation

化石墨烯烧蚀区域面积随脉冲个数和能量的变化趋势。与1030 nm波长激光烧蚀不同,氧化石墨烯表

面烧蚀区域大小并不随辐照的脉冲个数增加而变化。当入射激光脉冲能量固定时,烧蚀区域面积基本保持不变。这表明在257 nm激光辐照过程中,烧蚀区域表面的横向热扩散与沉积的脉冲能量无关。由于入射激光波长为紫外波段,单光子能量约为4.8 eV,材料烧蚀过程中主要以光化学^[20]方式为主,多脉冲辐照下氧化石墨烯表面含氧官能团被去除,材料在极短时间内大量电离,因此不会在氧化石墨烯薄膜面内形成相应的热量累积。图6详细对比了40 nJ激光烧蚀氧化石墨烯的表面形貌,可以发现在低脉冲个数辐照区域的边缘存在大量的纳米薄片。与1030 nm激光烧蚀区域形貌对比可知,随着脉冲个数的增加,257 nm激光辐照区域内部没有出现环形层状结构,这也进一步说明257 nm与1030 nm波长激光辐照过程中氧化石墨烯的烧蚀机制存在不同,1030 nm激光烧蚀氧化石墨烯在多脉冲辐照下存在激光能量的沉积与层间的热扩散,而257 nm激光烧蚀主要以光化学作用所导致的材料电离为主。

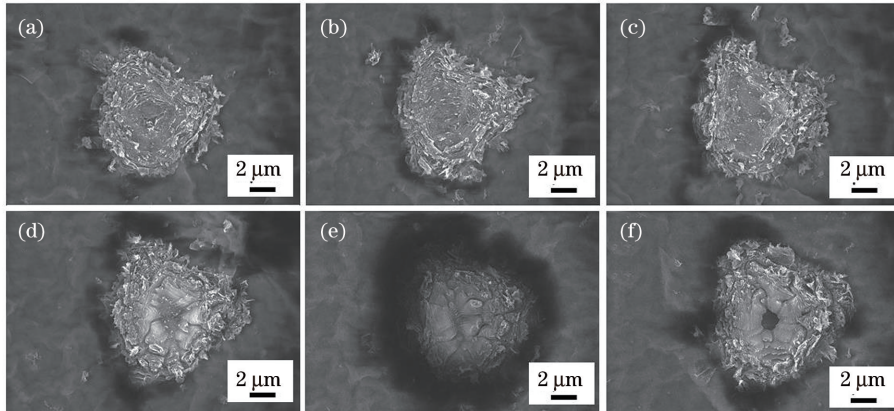


图6 257 nm 飞秒激光辐照氧化石墨烯表面烧蚀形貌。(a) 5 脉冲;(b) 20 脉冲;(c) 40 脉冲;(d) 60 脉冲;(e) 80 脉冲;(f) 100 脉冲

Fig. 6 Ablated surface morphology of graphene oxide by 257 nm femtosecond laser irradiation. (a) 5 pulses; (b) 20 pulses; (c) 40 pulses; (d) 60 pulses; (e) 80 pulses; (f) 100 pulses

3.2 表面纳结构成型特征研究

为了进一步研究飞秒激光辐照产生的纳结构形貌特征,采用激光线扫描方式在氧化石墨烯薄膜表面进行处理。图7为1030 nm和257 nm飞秒激光辐照下表面纳结构形貌,其中入射激光的脉冲能量均为30 nJ,扫描速度为10 mm/s。从图中可以发现,1030 nm波长激光辐照下形貌呈现条纹状结构且周期间隔约为800~900 nm,而257 nm波长激光辐照则产生随机分布的沟槽形貌结构。观察图7(c)、(f)中激光辐照氧化石墨烯的侧面形貌,1030 nm激光辐照产生的亚波长周期条纹纳结构为三维形貌,辐照区域相对未辐照的原始氧化石墨烯

表面在飞秒激光作用下膨胀。对比257 nm激光辐照产生的沟槽纳结构,其形貌特征呈现片状结构,并且相比于未辐照区域,257 nm激光作用区域的厚度明显减小,这再次表明纳结构形貌特征与入射激光的波长直接相关。在1030 nm波长的激光辐照过程中,辐照区域的氧化石墨烯表面含氧官能团被去除。同时,伴随着氧化石墨烯的还原,入射激光与还原氧化石墨烯表面等离子体(表面电磁波)发生干涉,干涉能量场刻蚀出条纹纳结构,其结构周期与干涉能量场的振动周期相同。而且周期纳结构的形成会进一步提升氧化石墨烯对入射激光能量的吸收,这种入射激光光场与纳结构的耦合作用使得周

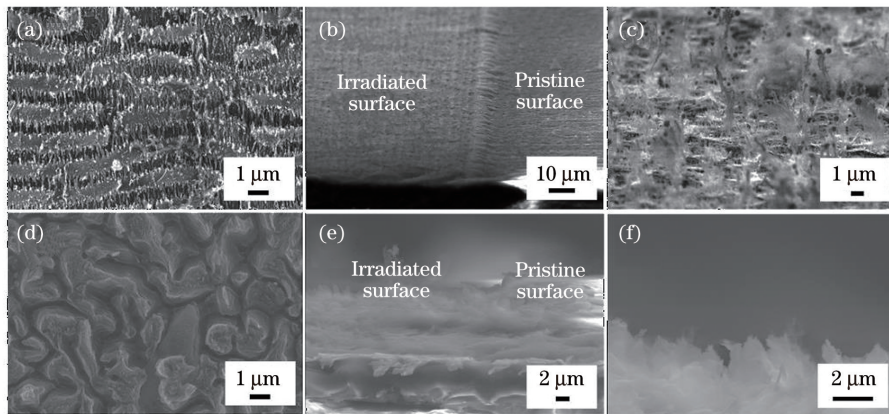


图 7 1030 nm 和 257 nm 激光辐照下纳结构表面与侧面形貌。(a) 1030 nm 激光辐照表面;(b) 1030 nm 激光辐照侧面;(c) 1030 nm 激光辐照放大图;(d) 257 nm 激光辐照表面;(e) 257 nm 激光辐照侧面;(f) 257 nm 激光辐照侧面放大图

Fig. 7 Surface and side morphology of nanostructures irradiated by 1030 nm and 257 nm laser . (a) Surface morphology irradiated by 1030 nm laser; (b) lateral morphology irradiated by 1030 nm laser; (c) enlarged lateral morphology irradiated by 1030 nm laser; (d) surface morphology irradiated by 257 nm laser; (e) lateral morphology irradiated by 257 nm laser; (f) enlarged lateral morphology irradiated by 257 nm laser

期条纹纳结构深度加深,形貌特征更加明显。而对于 257 nm 波长激光来说,光化学作用在激光辐照氧化石墨烯过程中起主导作用。光化学作用所导致的光机械效应更加明显,氧化石墨烯薄膜纳米片在 257 nm 波长激光作用下在极短时间内发生电离蚀除,从而形成沟槽微纳结构。此外,激光辐照氧化石墨烯的还原程度也与表面纳结构形貌相关。图 8 中拉曼光谱对比了 1030 nm 和 257 nm 激光辐照氧化石墨烯的表面特征峰峰位变化。氧化石墨烯的特征峰主要包括了 D 峰、G 峰和 2D 峰,其中 D 峰范围为 1350 cm^{-1} 左右,描述石墨烯碳网结构的内部缺陷; G 峰范围在 $1450\sim1600\text{ cm}^{-1}$ 之间,表明石墨烯层内声子振动模式;而范围在 $2450\sim2700\text{ cm}^{-1}$ 之间的 2D 峰位则可以反映氧化石墨烯的还原程度^[18,21]。

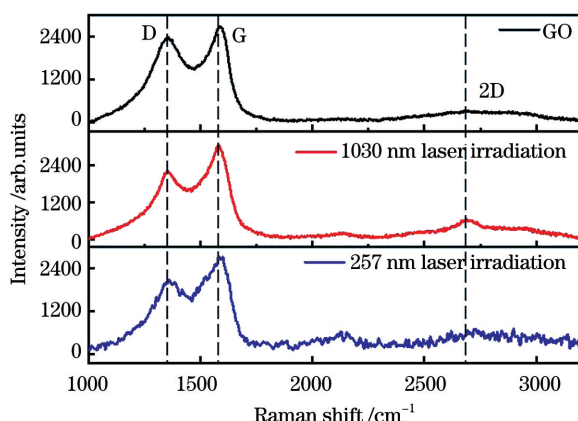


图 8 飞秒激光辐照氧化石墨烯的拉曼光谱

Fig. 8 Raman spectra of the graphene oxide by femtosecond laser irradiation

从图中可以看出,1030 nm 激光辐照产生的表面条纹纳结构相对于原始氧化石墨烯表面的 D 峰与 G 峰强度比(I_D/I_G)下降,2D 峰与 G 峰(I_{2D}/I_G)强度比增加。由还原氧化石墨烯的拉曼光谱峰位变化可知,1030 nm 激光作用后不仅使得表面形貌结构发生变化,而且碳网结构中碳原子轨道由 sp^3 杂化转变成 sp^2 杂化,实现了氧化石墨烯的还原。但 257 nm 激光辐照下表面纳结构的 2D 峰位强度却很明显,表明氧化石墨烯碳网结构中 sp^3 杂化并没有发生明显变化。拉曼光谱测试结果说明,在相同激光能量辐照下,1030 nm 激光相比于 257 nm 激光更有助于氧化石墨烯内部的碳网结构转变,氧化石墨烯的还原程度相对更高。

3.3 电化学阻抗测试与分析

利用飞秒激光微细刻划方法,在两种纳结构的还原氧化石墨烯薄膜上分别加工出指状电极。图 9 为 1030 nm 和 257 nm 激光辐照产生的含有不同表面纳结构的指状电极交流阻抗谱。从图中可以看出,带有条纹纳结构电极的接触电阻 $R_\Omega=40\ \Omega$,沟槽结构电极的接触电阻为 $154.7\ \Omega$,表明 1030 nm 激光辐照下还原氧化石墨烯的电极内阻比 257 nm 激光辐照下更小。其次,通过对两种纳结构电极的阻抗谱拟合可以获得相应的等效电路图,相比于沟槽结构电极的高频区谱图,条纹纳结构电极呈现半环形状,表现出明显的电荷转移过程。而对于低频区来说主要体现电极的扩散过程,条纹纳结构电极所对应的谱图斜线的斜率大于沟槽结构电极对应的谱图斜线斜率,表明 1030 nm 激光辐照产生的纳结

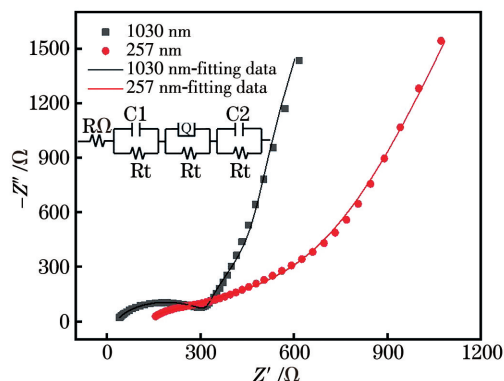


图 9 1030 nm 和 257 nm 飞秒激光辐照氧化石墨烯的电化学阻抗谱

Fig. 9 Electrochemical impedance spectra of graphene oxide irradiated by 1030 nm and 257 nm femtosecond laser
构有利于电极反应过程中的离子扩散。

4 结 论

氧化石墨烯在飞秒激光辐照下的表面纳结构的形成与入射激光参数直接相关。1030 nm 激光辐照氧化石墨烯过程中, 入射激光与表面等离激元发生干涉作用, 进而形成纳周期条纹结构。而 257 nm 激光辐照产生的沟槽微纳结构主要由光化学作用所致。通过对氧化石墨烯表面产生的纳结构的形貌与结构表征分析, 发现 1030 nm 激光辐照下氧化石墨烯的还原程度要高于 257 nm 激光辐照。基于电化学特性分析, 对比两种表面纳结构电极的阻抗谱, 发现具有条纹周期纳结构的电极的接触电阻小于沟槽纳结构电极的接触电阻。因此, 在入射激光能量相同时, 1030 nm 飞秒激光辐照更有助于氧化石墨烯的还原以及在微型电极方面的应用。

参 考 文 献

- [1] Novoselov K S, Geim A K, Morozov S V, et al. Two-dimensional gas of massless Dirac fermions in graphene[J]. *Nature*, 2005, 438(7065): 197-200.
- [2] Nair R R, Blake P, Grigorenko A N, et al. Fine structure constant defines visual transparency of graphene[J]. *Science*, 2008, 320(5881): 1308.
- [3] Allen M J, Tung V C, Kaner R B. Honeycomb carbon: a review of graphene[J]. *Chemical Reviews*, 2010, 110(1): 132-145.
- [4] Huang Y, Liang J, Chen Y. An overview of the applications of graphene-based materials in supercapacitors [J]. *Small (Weinheim an Der Bergstrasse, Germany)*, 2012, 8(12): 1805-1834.
- [5] Liu Y X, Dong X C, Chen P. Biological and chemical sensors based on graphene materials [J]. *Chemical Society Reviews*, 2012, 41(6): 2283-2307.
- [6] Bae S, Kim H, Lee Y, et al. Roll-to-roll production of 30-inch graphene films for transparent electrodes [J]. *Nature Nanotechnology*, 2010, 5(8): 574-578.
- [7] Novoselov K S, Geim A K, Morozov S V, et al. Electric field effect in atomically thin carbon films [J]. *Science*, 2004, 306(5696): 666-669.
- [8] Berger C, Song Z, Li X, et al. Electronic confinement and coherence in patterned epitaxial graphene[J]. *Science*, 2006, 312(5777): 1191-1196.
- [9] Wang S J, Geng Y, Zheng Q B, et al. Fabrication of highly conducting and transparent graphene films[J]. *Carbon*, 2010, 48(6): 1815-1823.
- [10] Wei Z, Wang D, Kim S, et al. Nanoscale tunable reduction of graphene oxide for graphene electronics [J]. *Science*, 2010, 328(5984): 1373-1376.
- [11] Yang D F, Bock C. Laser reduced graphene for supercapacitor applications [J]. *Journal of Power Sources*, 2017, 337(1): 73-81.
- [12] Yuan Y J, Li X. Femtosecond laser processing of graphene and its application [J]. *Laser & Optoelectronics Progress*, 2020, 57(11): 111414.
- [13] 原永玖, 李欣. 飞秒激光加工石墨烯材料及其应用 [J]. 激光与光电子学进展, 2020, 57(11): 111414.
- [14] Long J Y, Huang T, Ye X H, et al. Effects of low power CO₂ laser irradiation on structure of multilayer graphene[J]. *Chinese Journal of Lasers*, 2012, 39(12): 1206001.
- [15] 龙江游, 黄婷, 叶晓慧, 等. 低功率 CO₂ 激光辐照对多层石墨烯结构的影响 [J]. 中国激光, 2012, 39(12): 1206001.
- [16] Cui J L, Cheng Y, Zhang J W, et al. Femtosecond laser irradiation of carbon nanotubes to metal electrodes[J]. *Applied Sciences*, 2019, 9(3): 476.
- [17] Guo L, Jiang H B, Shao R Q, et al. Two-beam-laser interference mediated reduction, patterning and nanostructuring of graphene oxide for the production of a flexible humidity sensing device [J]. *Carbon*, 2012, 50(4): 1667-1673.
- [18] Kang S, Evans C C, Shukla S, et al. Patterning and reduction of graphene oxide using femtosecond-laser irradiation [J]. *Optics & Laser Technology*, 2018, 103: 340-345.
- [19] Trusovas R, Ratautas K, Račiukaitis G, et al. Reduction of graphite oxide to graphene with laser irradiation[J]. *Carbon*, 2013, 52: 574-582.
- [20] Kasischke M, Maragkaki S, Volz S, et al. Simultaneous nanopatterning and reduction of graphene oxide by femtosecond laser pulses [J]. *Applied Surface Science*, 2018, 445: 197-203.
- [21] Hummers W S Jr, Offeman R E. Preparation of

- graphitic oxide[J]. Journal of the American Chemical Society, 1958, 80(6): 1339.
- [20] Hua X G, Wei X, Zhou M, et al. Experimental study on mechanism of 355 nm ultraviolet laser polishing of Al_2O_3 ceramics[J]. Chinese Journal of Lasers, 2014, 41(12): 1203002.
华显刚, 魏昕, 周敏, 等. 355 nm 紫外激光抛光 Al_2O_3 陶瓷作用机理的实验研究[J]. 中国激光, 2014, 41(12): 1203002.
- [21] Arul R, Oosterbeek R N, Robertson J, et al. The mechanism of direct laser writing of graphene features into graphene oxide films involves photoreduction and thermally assisted structural rearrangement[J]. Carbon, 2016, 99: 423-431.

Nanostructure and Electrochemical Performance of Graphene Oxide by Irradiation of Femtosecond Laser

Li Qiang^{1,2}, Ding Ye^{1,2*}, Yang Lijun^{1,2**}, Wang Yang^{1,2}

¹ Key Laboratory of Micro-Systems and Micro-Structures Manufacturing, Ministry of Education, Harbin, Heilongjiang 150001, China;

² College of Mechatronics Engineering, Harbin Institute of Technology, Harbin, Heilongjiang 150001, China

Abstract

Objective Due to the advantage of high electrical conductivity, thermal conductivity, and superior surface area ratio, graphene has become the current research focus in the application of flexible energy storage and sensor. Comparing the chemical vapor deposition, mechanical exfoliation, and epitaxial growth, the direct reduction of graphene oxide (GO) can satisfy the demand for graphene production in the industrial field. Currently, the methods of GO reduction are chemical, thermal, and photon reductions. Based on reduction efficiency and cost-benefit, laser irradiation is an efficient way to remove the surface oxygen group for GO reduction without special physical and chemical conditions. Thus, laser reduction can be considered a highly effective method for graphene production. Some study has focused on different methods of GO through laser reduction, such as KrF excimer, ultraviolet, and femtosecond laser. Despite these investigations on GO reduction, simultaneous reduction and nanopattern of GO through laser irradiation are still challenging. To further investigate the morphology and structural properties of reduced GO, this study compares the morphology of the reduced GO with different nanostructures through femtosecond laser irradiation with 1030 nm and 257 nm. Besides, the influence of different laser-induced nanostructures on the electrochemical impedance will be discussed.

Methods GO can be obtained using Hummers methods. Different from graphene, surface oxygen-containing groups located at the surface and margin of GO nanosheets improve the hydrophilicity property. By the preparation of GO dispersion, spray coating was used to form a uniform GO film on the polyethylene terephthalate (PET) substrate. After that, a femtosecond laser with 1030 nm and 257 nm was irradiated on the GO surface to construct the nanostructure. The morphology and characteristics of nanostructure were compared to show the difference of GO through femtosecond laser irradiation. The all-solid-state interdigital micro-supercapacitors were constructed with the assistance of PVA/ H_2SO_4 to obtain the electrochemical performance of GO by femtosecond laser.

Results and Discussions The surface ablated morphology of GO using femtosecond laser irradiation was observed. The comparison results showed that the morphology evolution in GO has not followed the linear change with an increase in the incident laser energy and pulses number (Figs. 3 and 5). Under the 1030 nm laser irradiation, the ablated region of GO occurred in the layered annular structure, resulting from energy deposition and thermal diffusion. However, a large number of nanosheets located at the ablated margin of GO were obtained by 257 nm laser irradiation. The photochemical effect plays a significant role in laser irradiation. Two surface laser-induced nanostructures were further investigated to obtain the mechanism in the morphology evolution of GO (Fig. 7). Femtosecond laser-induced periodic surface structures (LIPSSs) with a high and low spatial frequency contributes to the surface plasmon polaritons (SPPs) on the GO surface. The coupling effect of SPPs and LIPSSs can result in the formation of nanostructure by 1030 nm femtosecond laser irradiation. The photomechanical effect induced by photochemical action is the main reason for the groove nanostructure's formation by 257 nm laser irradiation. Combined with the results of the Raman spectrum of GO (Fig. 8), the ratio of the intensity of D and 2D peaks

relative to that of G peak was calculated. Thus, the 1030 nm laser irradiation is essential for improving the transformation of graphite structure from sp^3 to sp^2 and removing surface oxygen-containing groups. Through the electrochemical impedance spectra (Fig. 9), the impedance spectra of different nanostructures induced by laser irradiation with 1030 nm and 257 nm display apparent distinct. The ohmic resistance value nanostructure with LIPSSs or stripe is $40\ \Omega$, which is lower than that of the nanostructure with groove morphology. According to the test data fitting, the nanostructure with LIPSSs or stripe morphology demonstrates the process of charge transformation at the high frequency and ion diffusion at the low frequency. The results suggested that the nanostructure by femtosecond laser irradiation with 1030 nm can improve the electrochemical action of micro-supercapacitors.

Conclusions In this study, the morphology and characteristics of GO nanostructures were investigated using femtosecond laser irradiation. Under the 1030 nm laser irradiation, the interference effect of SPPs and incident laser results in the formation of stripe nanostructure with the period of subwavelength. The groove nanostructure by 257 nm laser irradiation contributes to the photochemical effect. Based on the analysis of the Raman spectra of GO by femtosecond laser irradiation, the GO reduction level by 1030 nm femtosecond laser irradiation is higher than that of GO by 257 nm laser irradiation. Compared with the results of electrochemical impedance of different nanostructures by femtosecond laser irradiation, the GO nanostructure by 1030 nm laser irradiation improves the rate of ion diffusion of electrodes and decreases the ohmic resistance. This study will strengthen the practical application of simultaneous reduction and nanopatterning of GO by femtosecond laser in microelectronic devices.

Key words laser technology; femtosecond laser; graphene oxide; nanostructure; electrochemical performance

OCIS codes 320.7090; 350.3390; 320.2250